Effect of Selective Area Growth mask width on Multi-Quantum-Well Electroabsorption Modulated Lasers investigated by synchrotron radiation X-ray microprobe

Effect of Selective Area Growth mask width on Multi-Quantum-Well Electroabsorption Modulated Lasers investigated by Synchrotron Radiation X-ray Microprobe

Lorenzo Mino, Angelo Agostino, Simone Codato, Gema Martinez-Criado and Carlo Lamberti

Nuclear Instruments and Methods in Physics Research B
284 (2012) 6–9

Available online 16 September 2011

doi:10.1016/j.nimb.2011.09.009

Effect of Selective Area Growth mask width on Multi-Quantum-Well Electroabsorption Modulated Lasers investigated by synchrotron radiation X-ray microprobe

Lorenzo Mino [a,*], Angelo Agostino [b], Simone Codato [c], Gema Martinez-Criado[d] and Carlo Lamberti [a]

[a]*Department of Inorganic, Materials and Physical Chemistry, NIS Centre of Excellence and INSTM unit, University of Turin, Via P. Giuria 7, I-10125 Turin, Italy;*
[b]*Department of General and Organic Chemistry, NIS Centre of Excellence, University of Turin, C.so Massimo D'Azeglio 48, I-10125, Turin, Italy;*
[c]*Avago Technologies Italy S.r.l., Torino Technology Centre, Via G. Schiaparelli 12, 10148 Turin, Italy;*
[d]*ESRF, 6 rue Jules Horowitz, BP220, F-38043, Grenoble CEDEX, France.*

**Corresponding author: lorenzo.mino@unito.it*

Abstract
High performance optoelectronic devices require monolithic integration of different functions at chip level. This is the case of multi-quantum well (MQW) electroabsorption modulated laser (EML), employed in long-distance, high-frequency optical fiber communication applications, which is realized exploiting the selective area growth (SAG) technique. Optimization of the growth parameters is carried out by empirical approaches since a direct characterization of the MQW is not possible with laboratory X-ray sources, owing to the micrometer-variation of composition and thickness inherent to the SAG technique. In this work we combined micrometer-resolved photoluminescence with synchrotron radiation micrometer-resolved X-ray fluorescence to study the effect of different SAG masks on the electronic properties and chemical composition of the SAG MQW EML device.

Introduction
Nowadays the improvement of the frequency of transmission is one of the most relevant issues in the field of optical communication systems. To achieve this goal, the laser employed for the generation of the signals are normally based on Multi-Quantum Wells (MQW) quaternary III-V semiconductor alloys, which are deposited on suitable substrates by Metal-Organic Vapor Phase Epitaxy (MOVPE) [1]. Moreover the most advanced devices require the integration of two different functions at chip level: excellent results in the development of monolithic integration have been reached with the Selective Area Growth (SAG) technique [2; 3].
SAG exploits the perturbation of the growth fluxes induced by a dielectric mask (normally SiO_2): when the metal-organic precursors collide with the dielectric mask, they are deflected and they can migrate through the unmasked semiconductor where the growth can take place. In this way the reactive species coming from the gas phase are enriched by those deflected by the mask: the result is a variation in composition and thickness of semiconductors grown near (SAG region) and far (FIELD region) from the mask (see Figure 1).
Electroabsorption modulated lasers (EML) [4; 5], obtained by monolithic integration of an electroabsorption modulator (EAM) with a distributed feedback laser (DFB), are one of the most promising applications of SAG. A voltage modulation (-2V in our case) applied to the EAM switches it between an opaque and a transparent state by means of the Stark effect [6] and ensures the modulation of the DFB laser emission, allowing long-distance communications (up to 80 km) at high frequency (10 Gb/s).

In our investigations we considered SAG EML devices based on $Al_{xw}Ga_{yw}In_{1-xw-yw}As/Al_{xb}Ga_{yb}In_{1-xb-yb}As$ (compressive-strained well/tensile-strained barrier) MQW heterostructures grown on InP by MOVPE. We studied the effect of several masks showing different width of the SiO_2 stripes (10, 20 and 30 μm) and a fixed opening width of 30 μm between them. Using 800 μm-long stripes and 600 μm-long FIELD, two devices per couple of stripes can be potentially obtained after cleavage and processing (about 20000 in a 2-inches InP substrate).

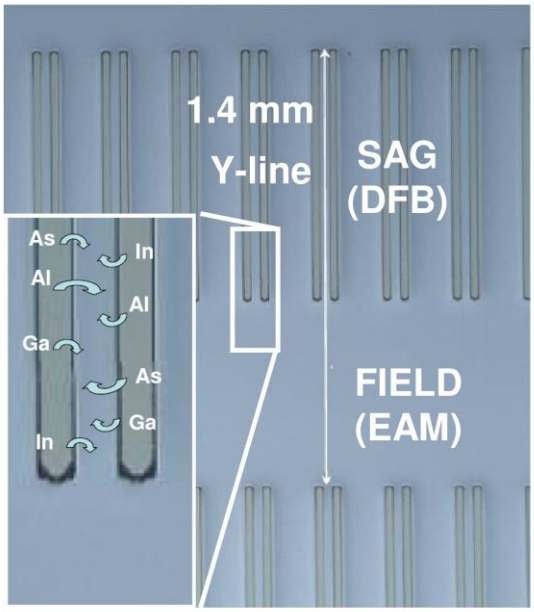

Figure 1. Optical micrograph of the InP substrate patterned with SiO_2 stripes allowing the SAG growth. In the inset a magnification of the interface between SAG and FIELD regions aiming to highlight the growth mechanism is reported. All the measurements have been acquired along a line parallel to the SiO_2 stripes and equidistant to them, labelled "Y-line" in the image.

Up to now trial and error procedures were adopted for the choice of growth parameters since the μm-variation of composition and thickness inherent to the SAG technique requires high brilliance X-ray microbeams in order to perform a proper characterization. These features are not achievable with conventional laboratory X-ray sources, therefore we moved to third generation synchrotron radiation sources and we decided to exploit the 5.3 μm × 1.7 μm X-ray beam available at the ID22 beamline [7] of the European Synchrotron Radiation Facility (ESRF).

Experimental

The samples were produced in the Avago Technologies Italy (Turin Technology Centre) laboratories with a commercial 6x2" Thomas Swan MOVPE reactor starting from $Al(CH_3)_3$, $Ga(CH_3)_3$, and $In(CH_3)_3$ as group-III sources, AsH_3 and PH_3 as group-V sources and H_2 as carrier gas. The SAG growths were obtained using three different masks with SiO_2 stripes featuring 10, 20 or 30 μm width and a fixed opening width of 30 μm between them. The MQW has been obtained with a repetition of 9 times of the $Al_{xw}Ga_{yw}In_{1-xw-ywAs}/Al_{xb}Ga_{yb}In_{1-xb-yb}As$ (compressive-strained well/tensile-strained barrier) heterostructure grown on InP. Photoluminescence experiments were performed with a dispersive Scantek instrument equipped with a He-Ne excitation source (resulting in a 2 μm diameter spot size), with a diffractive grating monochromator and an InGaAs photodetector.

ID22 beamline exploits the radiation produced by two different undulators: a standard linear undulator (U42), covering the energy range from 6 to 50 keV, and a second one (U23), which is a so-called in-vacuum linear undulator, inducing a much higher brilliance. Harmonic rejection is done by one single flat horizontally reflecting mirror and a Kohzu fixed-exit double crystal

monochromator is used with two different pairs of crystals: Si(111) for the low energy range (4-37 keV, employed in this work) and Si(311) for higher energies (7-72 keV).
The microprobe set-up is based on based on the Kirkpatrick–Baez (KB) mirrors [8], that allowed us to reach a spatial resolution of 1.7 μm (vertical) × 5.3 μm (horizontal). The KB mirrors have an efficiency of approximately 70% and, using both undulators together, when the current on the ESRF ring of about 200 mA, the photon flux measured in the focal spot is about 10^{12} photon/s at 13 keV. Different detectors such as a mini-ionization chamber and a Silicon Drift Detector (SDD) are used to monitor the intensity of the incoming beam and XRF signals. A video-microscope allows for the easy alignment of the sample and the microprobe set-up.

Results and Discussion
A μm-space resolved photoluminescence (μ-PL) was initially performed in order to verify the effect of the different masks on the energy gap of the material and to check the growth quality [9; 10]. A sampling step of 15 μm was adopted along a line parallel to the SiO_2 stripes and equidistant to them (hereafter "Y-line", see Figure 1).

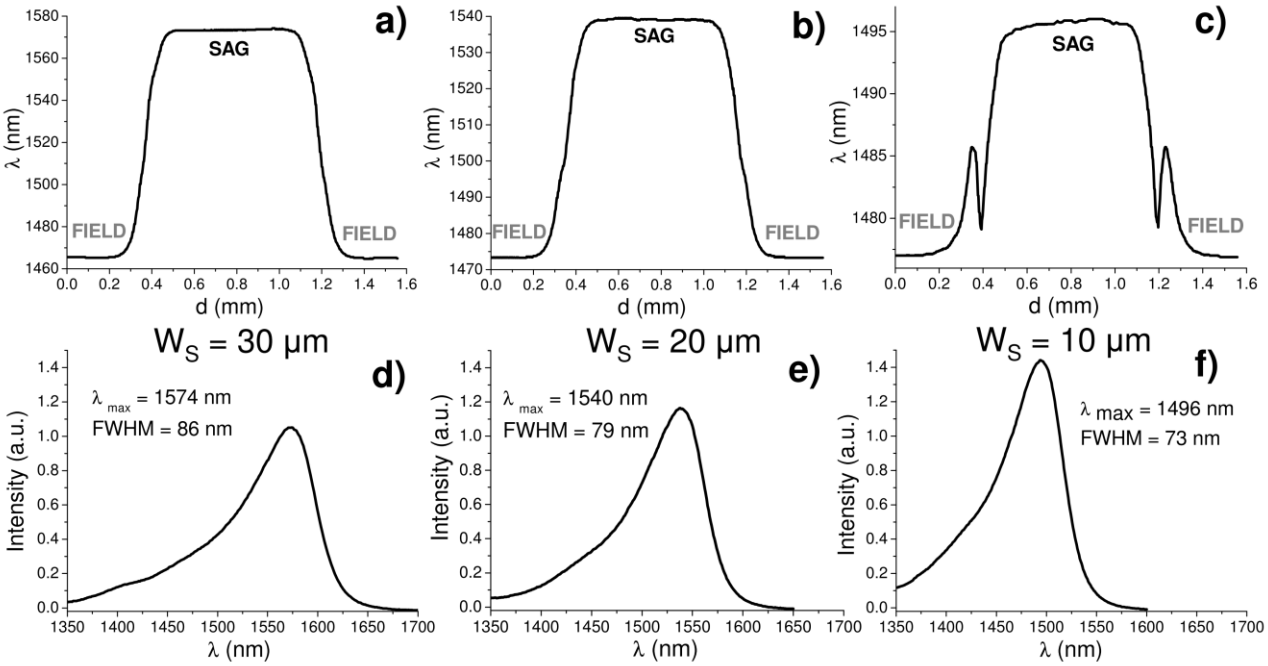

Figure 2. a) Wavelength corresponding to the maximum of emission for each PL spectrum collected on the sample with 30 μm stripes width (W_S = 30 μm) along a 1500 μm-long Y-line (see Figure 1) covering the complete mask from field to field. **b)** As part a) for the sample with W_S = 20 μm. **c)** As part a) for the sample with W_S = 10 μm. **d)** Complete PL spectrum for a point located in the centre of the SAG region of the sample with W_S = 30 μm. **e)** As part d) for the sample with W_S = 20 μm. **f)** As part d) for the sample with W_S = 10 μm.

In all the investigated materials the SAG region, which will host the DFB laser, emits at wavelengths optimized to exploit the third window of optic fibers (Figure 2a-b-c). Moreover the FIELD region shows a higher energy gap (lower λ) and therefore it is transparent to the radiation emitted by the laser when no voltage is applied. As expected, the difference in the energy gap between the two regions becomes smaller with decreasing the stripes width.
Considering the PL spectra moving from FIELD to SAG, the PL intensity becomes lower and the full width at half maximum (FWHM) becomes larger (see Table 1) reflecting a progressive degradation of the MQW crystalline quality: the worst values are found in the transition region. A similar trend is noticeable increasing the stripes width, as visible comparing Figures 2d, 2e and 2f. The phenomenon is related to lack of strain compensation, to a higher growth rate and to the

interference of precursors fluxes (coming from the gas phase and from the stripes) in the SAG region. Furthermore the precursors fluxes interference caused by the discontinuity created by the end of the SiO_2 stripes is responsible for the irregularity in the increase of the emission wavelength observed across the transition region (Figure 2a-b-c). This effect, particularly relevant for the 10 µm mask (see Figure 2c), causes growth waves which have been already highlighted in previous publications [11; 12]. It is also worth noticing that the wavelength corresponding to the maximum of emission is very similar for all the FIELD regions of the three different masks ($\Delta\lambda/\lambda < 0.01$, see Table 1).

Table 1. Wavelength corresponding to the maximum of emission (λ_{max}), emission intensity (I) and full width at half maximum (FWHM) for the µ-PL spectra acquired along the Y-line (see Figure 1) for the three masks with different stripes width (W_S). The first point (d = 0) is located in the center of the FIELD region whereas the last point (d=700) is located in the center of the SAG region.

W_S (µm)	d (µm)	Region	λ_{max} (nm)	I (a.u.)	FWHM (nm)
10	0	FIELD	1477	1.8	51
10	700	SAG	1496	1.4	73
20	0	FIELD	1473	1.7	53
20	150	FIELD	1473	1.7	53
20	220	INTERFACE	1475	1.7	54
20	300	INTERFACE	1496	1.7	60
20	370	INTERFACE	1525	1.1	82
20	450	INTERFACE	1538	1.1	78
20	550	SAG	1539	1.1	79
20	700	SAG	1540	1.1	79
30	0	FIELD	1464	1.8	64
30	700	SAG	1574	1.0	86

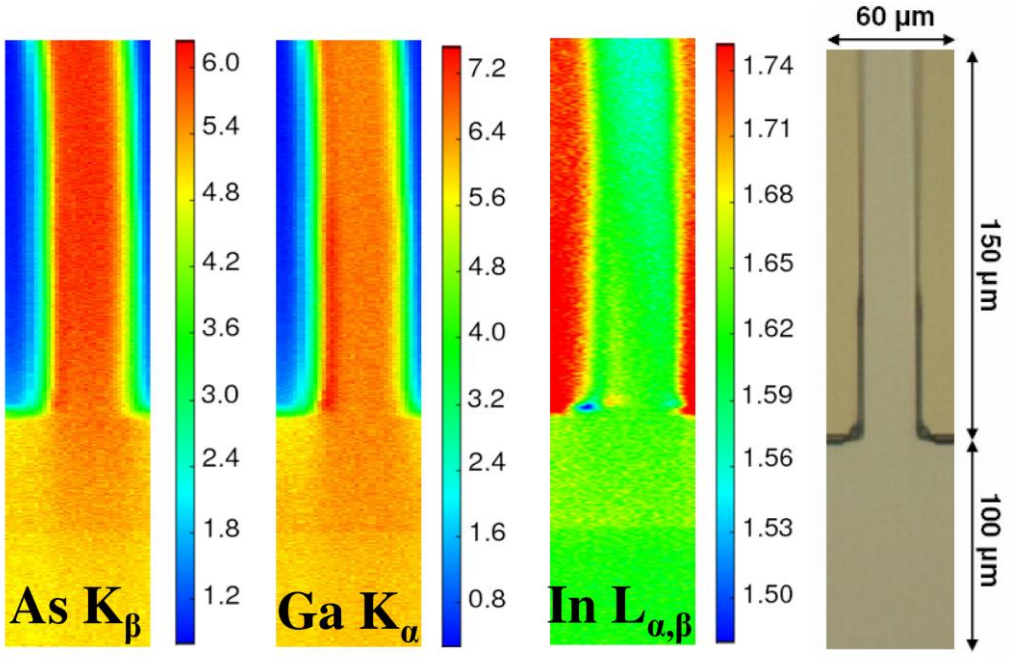

Figure 3. Spatial maps of the fluorescence counts of the principal element's lines (beam energy 17 keV). The optical micrograph on the right highlights the area which has been sampled. The use of As-K_β emission in place of the As-K_α was due to the fact that the As-K_α has a partial superimposition with Ga-K_β.

To correlate the change in the energy gap observed for the different masks with the corresponding change in chemical composition of the quaternary alloy, we exploited the synchrotron radiation X-ray microprobe available at the ESRF ID22 beamline to collect X-ray fluorescence (XRF) spectra. The XRF maps reported in Figure 3 reveal that Ga(K_α) and As(K_β) counts are higher in the SAG region owing to material enrichment caused by the SiO_2 stripes, which are visible as low counts regions, where no growth occurs. In the In($L_{\alpha,\beta}$) map the signal is biased by the emission coming from the InP substrate: the higher counts are noticeable in the region corresponding to the SiO_2 stripes since they are less effective than the MQW heterostructures in reabsorbing the emission coming from the substrate. Unfortunately, Al maps could not be acquired since the Al K-fluorescence at 1.5 keV was almost completely absorbed by the air and relegated to the background noise. These problems in having values above the detection limit prevented us from providing a complete quantitative analysis as recently performed for ternary SAG thin films [13].

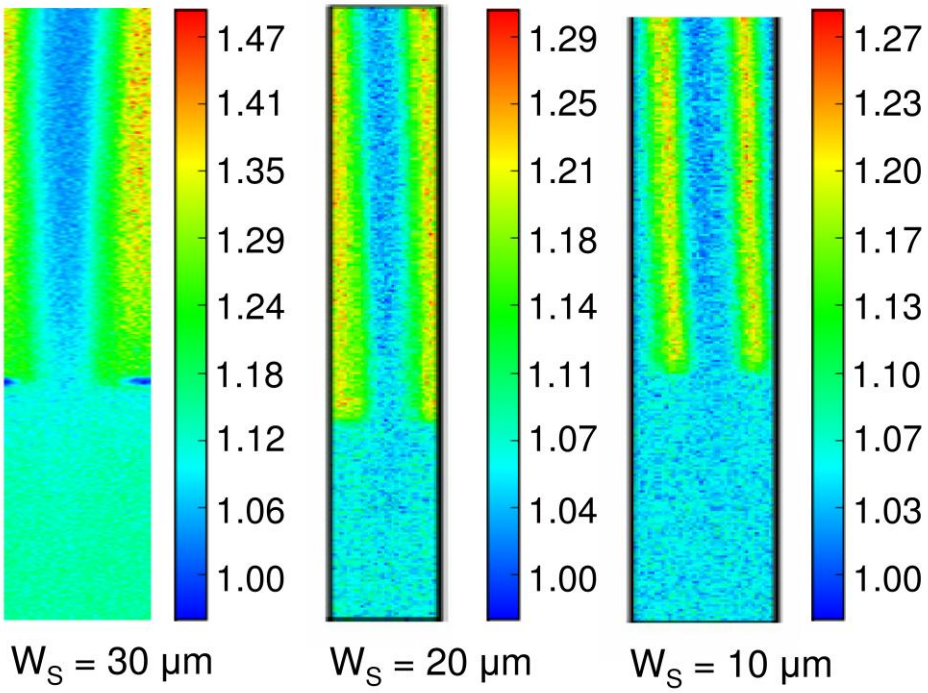

Figure 4. Spatial maps reporting the ratio between Ga(K_α) and As(K_β) counts that highlights the change in the average (between well and barrier) $Al_xGa_yIn_{1-x-y}As$ quaternary composition between SAG and FIELD regions for the different masks.

Nevertheless the gradient in the average well/barrier chemical composition can be investigated considering the maps reporting the ratio between Ga(K_α) and As(K_β) counts (Figure 4) in which it is clearly visible that in the FIELD region the Ga/As ratio is higher then in the SAG region. This means that the Ga content of the $Al_xGa_yIn_{1-x-y}As$ quaternary (averaged between wells and barriers) progressively increases along the Y-line by moving from SAG to FIELD. These results are in agreement with the models [2; 3; 14; 15] since the effective diffusion length (*D/k* coefficient, where *D* is the diffusion coefficient in the vapor phase while *k* depends upon the reactivity of the species on the crystal surface) of In is shorter with respect to those of Al and Ga [15; 16], therefore an In enrichment in the SAG region occurs. Moreover, as visible in Figure 4, the difference in the Ga/As ratio between the SAG and the FIELD regions decreases for the masks with smaller stripes confirming the trend already discussed for the µ-PL spectra.

Conclusions

The combination of µ-PL and µ-XRF allowed us to correlate the change in the energy gap observed for the different masks with the corresponding variation in chemical composition of the quaternary

heterostructures. In particular, although a complete quantitative XRF analysis was not possible, the study of the Ga/As maps provides a direct measurement of the effectiveness of SAG technique in modulating the chemical composition of III-V MQWs. Further improvements can be achieved if it will be possible to perform experiments in which also the Al K-fluorescence will be quantitatively detectable (e.g. in vacuum conditions).
Finally it is worth noticing that the investigated material is not an academic prototype, but is part of a device of industrial interest grown, processed and commercialized by Avago Technologies, therefore this characterization will provide useful information to improve the growth process, previously based only on a trial/error approach.

Acknowledgements. We are indebted with D. Gianolio, G. Agostini, A. Piovano, M. Truccato and S. Cagliero who have contributed to the XRF data collection during experiment MA-524.

References

[1]M. Razeghi, The MOCVD Challenge: Volume 2: A Survey of GaInAsP-GaAs for Photonic and Electronic Device Applications, IoP Publishing ltd, London, 1995.
[2]M. Gibbon, J.P. Stagg, C.G. Cureton, E.J. Thrush, C.J. Jones, R.E. Mallard, R.E. Pritchard, N. Collis, A. Chew, Semicond. Sci. Technol. 8 (1993) 998.
[3]N. Dupuis, J. Decobert, P.Y. Lagree, N. Lagay, F. Poingt, C. Kazmierski, A. Ramdane, A. Ougazzaden, J. Appl. Phys. 103 (2008) 8.
[4]R.A. Salvatore, R.T. Sahara, M.A. Bock, I. Libenzon, IEEE J. Quantum Electron. 38 (2002) 464.
[5]M. Meliga, R. Paoletti, C. Coriasso, Uncooled Laser Sources for Plug and Play Transceivers for Datacom and Telecom Applications. in: T. Shinji, B. Jens, L. Yi, (Eds.), Optoelectronic Materials and Devices for Optical Communications, Proceedings of the SPIE, Invited talk at the APOC conference, Shangai (China), 2005, pp. 382.
[6]D.A.B. Miller, D.S. Chemla, T.C. Damen, Phys. Rev. Lett. 53 (1984) 2173.
[7]A. Somogyi, R. Tucoulou, G. Martinez-Criado, A. Homs, J. Cauzid, P. Bleuet, S. Bohic, A. Simionovici, J. Synchrot. Radiat. 12 (2005) 208.
[8]C. Riekel, Rep. Prog. Phys. 63 (2000) 233.
[9]S. Sanguinetti, M. Guzzi, M. Gurioli, Accessing Structural and Electronic Properties of Semiconductor Nanostructures via Photoluminescence. in: C. Lamberti, (Ed.), Characterization of Semiconductor Heterostructures and Nanostructures, Elsevier, Amsterdam, 2008, pp. 175.
[10]C. Lamberti, Comput. Phys. Commun. 93 (1996) 82.
[11]L. Mino, D. Gianolio, G. Agostini, A. Piovano, M. Truccato, A. Agostino, S. Cagliero, G. Martinez-Criado, S. Codato, C. Lamberti, Adv. Mater. 22 (2010) 2050.
[12]L. Mino, D. Gianolio, G. Agostini, A. Piovano, M. Truccato, A. Agostino, S. Cagliero, G. Martinez-Criado, F. d'Acapito, S. Codato, C. Lamberti, Small 7 (2011) 930.
[13]L. Mino, A. Agostino, S. Codato, C. Lamberti, J. Anal. At. Spectrom. 25 (2010) 831.
[14]J.E. Greenspan, C. Blaauw, B. Emmerstorfer, R.W. Glew, I. Shih, J. Cryst. Growth 248 (2003) 405.
[15]J. Decobert, N. Dupuis, P.Y. Lagree, N. Lagay, A. Ramdane, A. Ougazzaden, F. Poingt, C. Cuisin, C. Kazmierski, J. Cryst. Growth 298 (2007) 28.
[16]N. Dupuis, J. Decobert, P.Y. Lagree, N. Lagay, C. Cuisin, F. Poingt, A. Ramdane, C. Kazmierski, IEE Proc.-Optoelectron. 153 (2006) 276.